Polymer 51 (2010) 3303–3314

Contents lists available at ScienceDirect

Polymer

journal homepage: www.elsevier.com/locate/polymer

Mono- or bidisperse nanorods mixtures in diblock copolymers

Linli He [a], Linxi Zhang [b,*], Haojun Liang [c]

[a] Department of Physics, Zhejiang University, Hangzhou 310027, PR China
[b] Department of Physics, Wenzhou University, Wenzhou 325027, PR China
[c] Department of Polymer Science and Engineering, University of Science and Technology of China, Hefei, 230026, PR China

ARTICLE INFO

Article history:
Received 18 September 2009
Received in revised form
12 April 2010
Accepted 15 May 2010
Available online 24 May 2010

Keywords:
Bidisperse nanorods mixture
Dissipative particle dynamics
Self-assembly

ABSTRACT

Mixtures of diblock copolymers (DBCPs) and mono- or bidisperse nanorods (NRs), are systematically investigated via dissipative particle dynamics simulations. For the mixtures of DBCPs and monodisperse NRs, we investigate the effects of the nanorod (NR) volume fraction, NR length, and interaction strength between blocks and NRs on the self-assembly of the composites. For the mixtures of DBCPs and bidisperse NRs in which the NRs are different in length, the binary NRs with varied compositions can induce various morphological transitions, as well as present the uniform orientations and discriminative distributions. The inherent mechanism for driving such rich phase behaviors can be further exploited on the basis of considering the enthalpic and entropic effects. The results provide some guidelines for engineering nanocomposites with the desired morphologies and functions.

1. Introduction

The self-assembly of organic polymers and inorganic filler particles into nanostructured composites can facilitate the development of novel biomimetic [1], photonic [2], and electronic [3,4] materials. Block copolymer/particle mixtures can constitute ideal self-assembling systems for creating high-performance nanocomposites, since the microphase separation of block copolymers can be harnessed to "template" the organization of the particles into various arrangement modes, such as nanoplanes, − wires, or −spheres [5]. However, the particles are not passive and also can alter both the orientation [6,7] and the morphology [8–11] of the copolymers microdomains. Therefore, the observed final microstructures of the nanocomposites will depend on the loaded particle size, shape, species and volume fraction, the composition and structure of the copolymers, and the interaction energies between the different components [12–14].

Recently, the phase behaviors of mono- or bidisperse nanoparticles (NPs) incorporated in block copolymers have been extensively studied by theories [15–20], experiments [21–23], and simulations [24,25]. Thompson et al. combined the self-consistent field (SCF) and density functional theories (DFT) to investigate the mesoscopical self-assembly of DBCPs/mono-disperse NPs mixtures [15,16]. In their following study, they also investigated the phase behaviors of bidisperse NPs mixtures in asymmetric DBCPs, and mainly discussed the entropic contributions involving all the different components [18–20]. Experimentally, Bockstaller et al. investigated the self-assembly of bidisperse NPs mixtures in symmetric lamellar DBCPs and found that the NPs of larger size were localized in the center of the preferred domains and those of smaller size were concentrated at the blocks interface in the same domains [22], consistent with theoretical [18–20] and simulation [25] results. However, compared with the isotropic spherical NPs, the investigations on the phase behaviors of anisotropic NRs in block copolymers are very scarce [26–34], especially for the bidisperse NRs mixture case. The situation for the copolymer/NR mixtures becomes much more peculiar because of the liquid crystalline phases of NRs [35–37]. The high-aspect-ratio particles, such as rods, can result in polymer nanocomposites processing superior optical and mechanical properties relative to polymers reinforced with an equivalent volume fraction of spherical particles [38]. Peng et al. showed that when low-volume fractions of nanoscale rods were immersed in a binary, phase-separating blend, the rods self-assembled into needlelike, percolating networks. These extensive networks could potentially improve both the mechanical and electrical properties of the copolymer/NR mixtures [30].

In our previous studies [33,34] on the phase behaviors of the monodisperse NRs incorporated in symmetric/asymmetric DBCPs melts, the NRs can tend to aggregate for the micelles formation, derived from the affinity between NRs. By varying the NR volume fraction, length, radius, and the polymer-NR interaction, we systematically analyzed the novel morphology and self-assembly of

* Corresponding author.
E-mail address: lxzhang@zju.edu.cn (L. Zhang).

0032-3861/$ – see front matter © 2010 Elsevier Ltd. All rights reserved.
doi:10.1016/j.polymer.2010.05.026

the composites. In this report, we describe a simulation on the self-assembly of mono- or bidisperse NRs incorporated in symmetric/asymmetric DBCPs. Particularly, we conduct the first investigations into the mixtures of DBCPs and bidisperse NRs that differ in length. Different from our previous studies [33,34], the choose of the large repulsive interaction between NRs can avoid the aggregates of NRs and as well as can highly improve the orientations of NRs. The phase structures of the mixtures, NRs' position distributions and spatial orientations will be exploited in detail. These results illustrate that the self-assembly in systems composed of block copolymers and anisotropic NRs can be utilized to create novel, spatially organized nanocomposites.

2. Theory and model

In 1992, Hoogerbrugge and Koelman [39] proposed a new simulation technique referred to as dissipative particle dynamics (DPD), appropriate for the investigation of the generic properties of macromolecular systems. Within the DPD approach [39,40], the fluid particles are coarse grained into 'beads' or DPD particles, which interact with each other via conservative, dissipative, and random forces.

$$\overrightarrow{F}_{ij}^{C} = a_{ij}\omega(r_{ij})\hat{r}_{ij} \tag{1}$$

$$\overrightarrow{F}_{ij}^{D} = -\gamma\omega^2(r_{ij})\left(\hat{r}_{ij}\cdot\overrightarrow{v}_{ij}\right)\hat{r}_{ij} \tag{2}$$

$$\overrightarrow{F}_{ij}^{R} = \sigma(\Delta t)^{-1/2}\omega(r_{ij})\xi_{ij}\hat{r}_{ij} \tag{3}$$

The conservative force $\overrightarrow{F}_{ij}^{C}$ is the soft repulsion acting along the intermolecular vector, where a_{ij} is a maximum repulsion between beads i and j; and $\overrightarrow{r}_{ij} = \overrightarrow{r}_i - \overrightarrow{r}_j$, $r_{ij} = |\overrightarrow{r}_{ij}|$, $\hat{r}_{ij} = \overrightarrow{r}_{ij}/r_{ij}$; $\omega(r)$ is a r-dependent weight function, for which we adopt the commonly used form

$$\omega(r) = \begin{cases} 1 - \mathrm{r}/\mathrm{r_C} & r_{ij} < r_c \\ 0 & r_{ij} \geq r_c \end{cases} \tag{4}$$

The other two forces ($\overrightarrow{F}_{ij}^{D}$ and $\overrightarrow{F}_{ij}^{R}$) act as a heat sink and a heat source, respectively, which effectively combine to thermostat the system, where $\overrightarrow{v}_{ij} = \overrightarrow{v}_i - \overrightarrow{v}_j$; and ξ_{ij} is a symmetric random variable with zero mean and unit variance, and is uncorrelated for different times and different particle pairs. The fluctuation-dissipation theorem requires that the friction coefficient γ and the noise amplitude σ are related through the relation

$$\sigma^2 = 2\gamma k_B T \tag{5}$$

where k_B is Boltzmann's constant. It is convenient to use reduced units in DPD [41]. The unit of length is defined by the cutoff radius r_c, the unit of mass is defined by the mass m of the particles (which are chosen to be the same for all the particles), and the unit of energy is defined by k_BT. Referring to the studies by Groot [41], we set $\gamma = 6.57$, so $\sigma = 3.62$ according to Eq. (5). Additionally, for the polymers, the spring force $\overrightarrow{f}_i^{s}$, which acts between the connected beads in a chain, has the form of

$$\overrightarrow{f}_i^{s} = \sum_j C\overrightarrow{r}_{ij} \tag{6}$$

where C is a harmonic type spring constant for the connecting pairs of beads in a polymer chain, chosen to be equal to 4 here (in terms of k_BT).

According to the approach taken by previous studies [42–44] in the DPD simulation, rigid particles also can be modeled from the constructed DPD beads. Similarly, in our study, the rigid NR is composed of a number of DPD beads N_b, with a fixed distance D_{b-b} between consecutive beads. Hence, the real length of a NR can be calculated by $L_r = (N_b - 1) \times D_{b-b}$ [42]. In order to avoid undesired penetration of fluid particles into NRs and overlap between NRs, the number density of the DPD beads in a NR is larger than the number densities of the A/B block in the fluid. Here, D_{b-b} is fixed at 0.3 and the NR length L_r ranges from 0.3 to 6.9. Hence, the ratio range of L_r/L_0 (NR length/period length of DBCPs) is about 0.06–1.5, comparing with the experimental ratio of L_r/L_0 = 50 nm/90 nm = 0.56 [27].

All DPD beads interact with each other via the same conservative, dissipative, and random forces, according to Eqs. (1)–(3). For the fluids, the Newton equations for particles' positions and velocities are solved by a modified version of the velocity Verlet algorithm [42]. Then for NRs, a constraining routine is used to keep the inner particles aligned and equidistant during the simulation. In short, the forces on the first and the second half part of a NR are converted into two net forces, which directly act on the two end DPD particles [42], and the equations of motion for these two DPD particles are solved, using the standard shake routine to keep them at a fixed distance. The positions of the N_p-2 intermediate DPD particles are then readily calculated by a linear interpolation at the end of each time-step [42].

Our model system consists of the mixtures of symmetric/asymmetric DBCPs (represented by A_5B_5/A_3B_7) and NRs (mono- or bidisperse). There are three types of DPD particles in our system represented by A, B, and R. The repulsion parameters a_{ij} between particles are chosen according to [41].

$$a_{ii}\rho = 75k_BT, \tag{7}$$

$$a_{ij} \approx a_{ii} + 3.27\chi_{ij}(\rho = 3) \tag{8}$$

$$a_{ij} \approx a_{ii} + 1.45\chi_{ij}(\rho = 5) \tag{9}$$

where a_{ii} is the repulsion parameter between particles of the same type. We have used density $\rho = 5$, hence the repulsion parameter $a_{ii} = 15$, and a_{ij} is obtained according to Eqs. (7) and (9). Correspondingly, the values of a_{ij} between A, B, and R DPD particles, are given by $a_{AA} = a_{BB} = 15$, $a_{AB} = a_{RR} = 30$, $a_{AR} = 15$, and the variable a_{BR}. Initially, fluid particles are arranged in a face-centered-cubic (fcc) lattice via spring forces, and NRs are randomly dispersed in the fluids. Periodic boundary conditions are applied in all three directions.

3. Results and discussion

Firstly, we check our compiled DPD program by calculating the bulk morphologies and period lengths for DBCPs (A_5B_5 and A_3B_7), and the results are consistent with that from DPD module in Material Studio software (from Accelrys, Inc.). However, the complex models in Material Studio software, such as rigid rods, are unrealizable. Then, the periodical boundary condition has been adopted to mimic a practical system, since the size effect in simulation may also exist. To eliminate the size effect and select the suitable size for our simulation, we calculate the bulk period lengths L_0 of A_5B_5 for five systems with different sizes of $7 \times 7 \times 7$, $9 \times 9 \times 9$, $11 \times 11 \times 11$, $13 \times 13 \times 13$, and $15 \times 15 \times 15$ DPD units. The corresponding values of L_0 are 5.1, 4.61, 4.60, 4.61, and 4.61, indicating that the size effect has been essentially eradicated for the box of $9 \times 9 \times 9$ DPD units. The same calculation for A_3B_7 also

verifies the adaptability of 9 × 9 × 9 DPD units system. For easy to compare, in following discussion, we focus on the 9 × 9 × 9 DPD units systems, containing about 3645 DPD fluid particles for the density of $\rho = 5$.

3.1. A_5B_5 and monodisperse NRs mixtures

For the case of monodisperse NRs, we focus on the mixtures of symmetric DBCPs A_5B_5 and A-preferential NRs with $a_{AR} = 15$ and $a_{BR} = 20$. Firstly, we investigate the effects of the NR length L_r and NR volume fraction ϕ_r on self-assembled structures of the mixtures. For the short NRs with $L_r = 1.5$, when $\phi_r = 8\%$, 32%, 48% and 64%, the induced morphological transition of the systems follows as $5L \rightarrow L + C \rightarrow C \rightarrow E$ shown in Fig. 1. For the long NRs with $L_r = 5.7$, when $\phi_r = 8\%$, 24%, 48% and 64%, the corresponding morphological transition is $5L \rightarrow 3L \rightarrow C \rightarrow E$ shown in Fig. 2. Here, $5L$ and $3L$, $L + C$, C, and E represent the four and two AB interfaces lamellar, lamellar/cylindrical mixed, cylindrical, and elliptic structures, respectively. Due to the preferential affinity to A blocks, the NRs are distributed selectively within the A phase domains. As shown in Figs. 1(b1–b4) and 2(b1–b4), the NR concentrations can further characterize the NRs' distributions and different nanostructures of the mixtures. These observations show the rich self-assembly behaviors of the mixtures under different NR lengths L_r and different volume fractions ϕ_r. In addition, the similar morphological transition for 13 × 13 × 13 DPD units systems is also obtained: $7L \rightarrow 5L \rightarrow C$ shown in Fig. 2(c1–c3). It indicates that the simulated system with the size of 9 × 9 × 9 DPD units is suitable not only for the pure DBCPs melts but also for the melts blended with NRs particles. Hence, all results in the following discussions are based on the calculations for 9 × 9 × 9 DPD units systems.

We construct an approximate phase diagram of the NR length L_r versus NR volume fraction ϕ_r as plotted in Fig. 3. Besides the five phases mentioned above: $5L$, $3L$, $L + C$, C, and E, we observe the spherical structure (S) represented by the solid circles in phase diagram. From the phase diagram we can see that the formation of spherical structure (S) requires a shorter NR length L_r with a larger volume fraction ϕ_r. According to the results of spherical nanoparticles (NPs) dispersed in the cylindrical forming DBCPs ($f_a = 0.37$) [8], an increase in the size of A-preferential NPs with fixed volume fraction ϕ_p, equivalently enhances the effective A composition of the chain (f_a), leading to morphological transitions from cylindrical (C) to lamellar (L). Here, for the case of lamellar forming DBCPs blended with A-preferential NRs, by varying the NR length L_r with NR volume fraction ϕ_r, a series of phase transitions are also observed. To the limit of NR length of $L_r = 0.3$ (i.e., consisted by only one DPD bead), with increasing ϕ_r, the typical morphological transition of $L \rightarrow C \rightarrow S$ is observed, which is equivalent to improve A block composition f_a, according to theoretically predicted phase diagram for pure DBCPs [45]. In comparison to the isotropic NPs, besides the phase transition of $L \rightarrow C \rightarrow S$, we also observe the lamellar/cylindrical mixed phase ($L + C$) and elliptical-shaped phase (E), originating from the effects of the anisotropic NRs' additional orientation. In other words, the anisotropy of loaded particles greatly influences the self-assembled structural orientation of diblocks. This is the reason why the formation of spherical structure (S) is only restricted to the short NRs (e.g., $L_r = 0.3$ and 0.9 in phase diagram), and not observed for slightly long NRs with highly NR volume fraction.

In addition, a close look at Figs. 1 and 2 reveals that there are some specific structures, in which the NRs are distributed uniformly in a hexagonal way shown in Fig. 1(a3–b3) and 2 (a2–b2). Meanwhile, these specific structures are marked out by line frame in the phase diagram shown in Fig. 3. On the whole, for short NRs with distributed hexagonally, the NR volume fraction ϕ_r required is relatively higher than that for long NRs. However, for the intermediate cases, such as $L_r = 3.9$ and 4.5, the structures with NRs distributed hexagonally are not observed, which will be explored later in detail. These observations indicate that the two key parameters (L_r and ϕ_r) not only affect the general morphology of the mixtures but also directly influence the phase behaviors of NRs in microphase separated DBCPs, such as the NRs' position distribution and spatial orientation.

In order to quantitatively present the NR spatial orientation within the diblocks, we calculate the average NR orientation with respect to a certain direction (i.e., z axis) as follows:

$$\langle P(\cos\theta)\rangle = \left\langle \left(3\cos^2\theta - 1\right)/2 \right\rangle \tag{10}$$

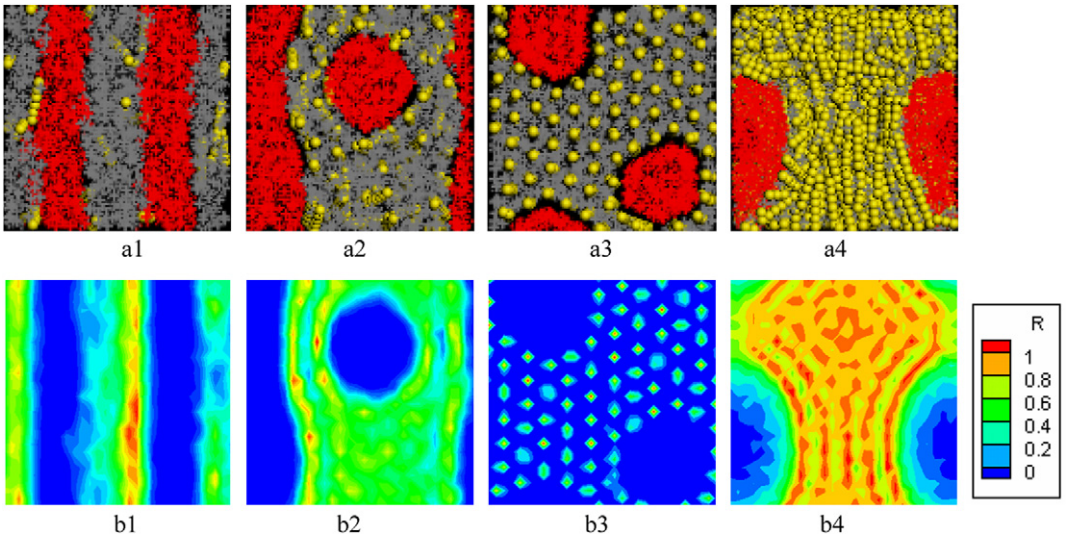

Fig. 1. Morphologies and NR concentrations for A_5B_5 and monodisperse NRs mixtures. The NR length $L_r = 1.5$ and varied NR volume fraction $\phi_r = 8\%$, 32%, 48% and 64% in (a1–a4). Here A/B blocks are presented in gray/red, and NRs are shown in yellow. The view plane is parallel to the NR orientation in Fig. 1a1 and a4, while the view plane is perpendicular to the NR orientation in Fig. 1a2 and a3. The legend represents the NRs concentration distribution with different colors (For interpretation of the references to colour in this figure legend, the reader is referred to the web version of this article).

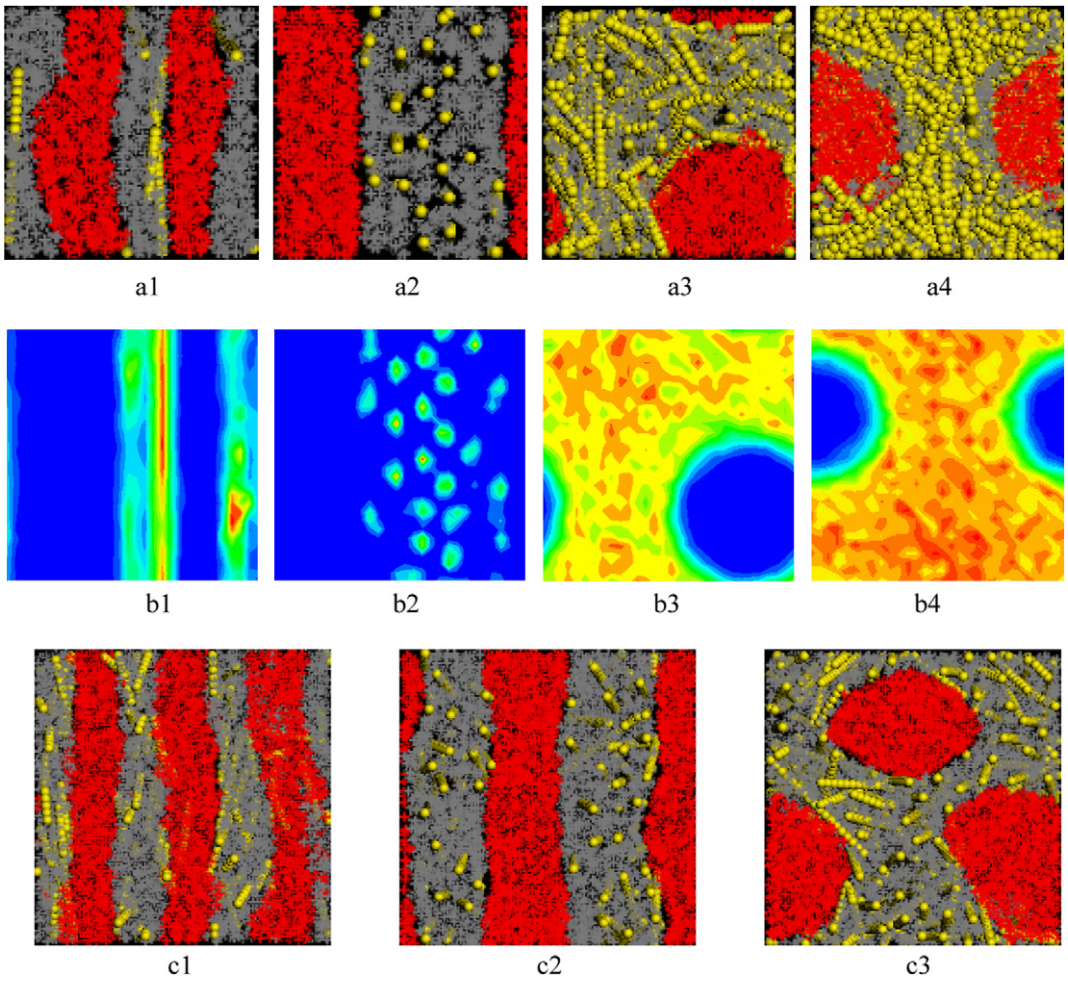

Fig. 2. Morphologies and NR concentrations for A_5B_5 and monodisperse NRs mixtures. The NR length $L_r = 5.7$ and varied NR volume fractions $\phi_r = 8\%$, 24%, 48% and 64% in (a1–a4). The morphologies for 13 × 13 × 13 DPD units systems are also shown in (c1–c3), corresponding to 9 × 9 × 9 DPD units systems in (a1–a3).

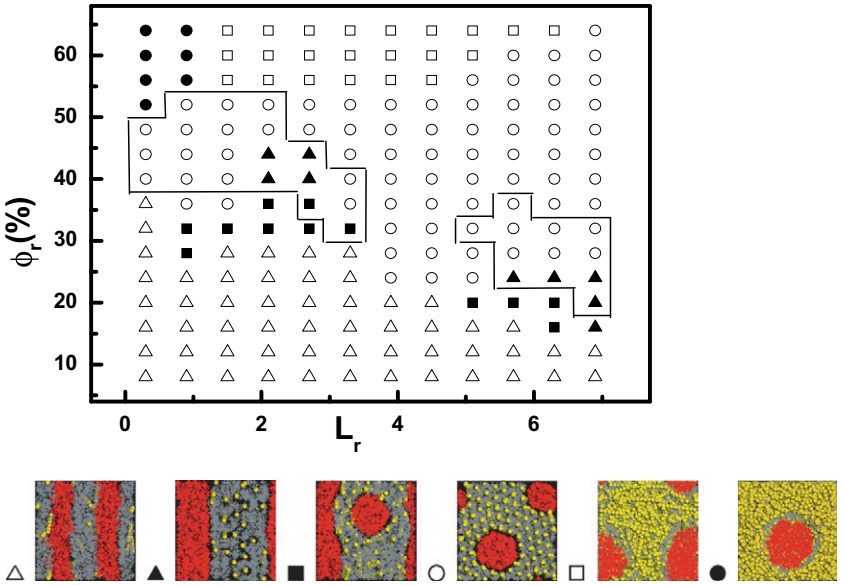

Fig. 3. The phase diagram for A_5B_5 and monodisperse NRs mixtures with different NR lengths L_r and different NR volume fractions ϕ_r. Graphic symbols represent ordered morphologies: △ = 5*L*, ▲ = 3*L*, ■ = *L* + *C*, ○ = *C*, □ = *E*, and ● = *S*. The points in line frame represent hexagonally uniform NR distributions.

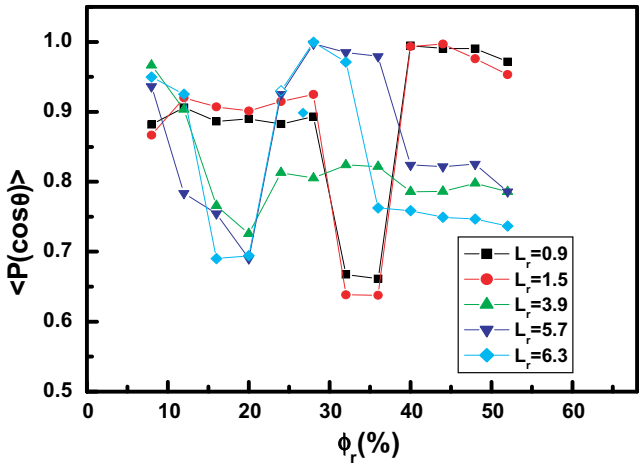

Fig. 4. The average NR orientation $<P(\cos\theta)>$ as a function of the NR volume fraction ϕ_r for A_5B_5 and monodisperse NRs mixtures.

$\langle P(\cos\theta)\rangle$will take values of −0.5, 0, and 1 for segments that are perpendicular, randomly oriented and parallel to the z axis [33,34]. Fig. 4 shows the average NR orientation $\langle P(\cos\theta)\rangle$ as a function of the NR volume fraction ϕ_r for the cases of $L_r = 0.9$, 1.5, 3.9, 5.7, and 6.3. We find that with the increase of ϕ_r, the values of $\langle P(\cos\theta)\rangle$ for different NR lengths L_r all undergo a sharp decrease, forming a "valley" on the curves. After the "valley", the values of $\langle P(\cos\theta)\rangle$ basically all experience an abrupt increase about at $\phi_r = 40\%$ for $L_r = 0.9$ and 1.5, and $\phi_r = 24\%$ for $L_r = 5.7$ and 6.3, while it is not obvious for $L_r = 3.9$. The higher the value of $\langle P(\cos\theta)\rangle$ is, the more uniform orientation the NRs exhibit in the polymer matrix. The higher values of $\langle P(\cos\theta)\rangle$ after the "valley" in Fig. 4 correspond exactly the special structures (with NRs distributed hexagonally) inside line frame box in Fig. 3. This similar orientation behaviors for $\langle P(\cos\theta)\rangle$ are also monitored in our previous study [34], which had been well interpreted by calculating the interaction energy among the NRs to reflect the particle–particle relative distances. With a low-volume fraction of NRs, the NRs tend to dispersely distribute in A-preferential domains, and the spatial confinement from the lamellar DBCPs strongly orientates the NRs behaviors, requiring a high value of $\langle P(\cos\theta)\rangle$. With an increase in NR volume fraction ϕ_r, the instinctive aggregates as a result of NRs' anisotropy, drive the NRs to mainly distribute in A domains with a relative free orientation, resulting in the "valley" on the curves of $\langle P(\cos\theta)\rangle$. Then, with a higher loading concentration of NRs, the competitions between the confinements governed by phase separated DBCPs domains, the liquid crystalline behaviors governed by rods, and the repulsive interactions between NRs, cooperatively optimize the orientation of NRs and require a high value of $\langle P(\cos\theta)\rangle$ again. A further loading of NRs naturally leads to a decrease in $\langle P(\cos\theta)\rangle$, dominated by the strong repulsions between a large number of NRs. In addition, for the special case of $L_r = 3.9$ (line + symbols in green), there is no significant increase in $\langle P(\cos\theta)\rangle$ curve after the "valley", which also directly reflects the results that the special structures with NRs distributed hexagonally are not observed for $L_r = 3.9$ and 4.5 in Fig. 3. Presumably, there is a matching problem between NR length and structural period of DBCPs. Only the best matching among limited structural period of diblocks, NR length and volume fraction, one can contribute to the NRs distributed hexagonally. Substantially, the unique phase behaviors of diblock/NR mixtures can be rationalized on the basis of considering the enthalpic and entropic effects involving all of the species, A, B blocks and NRs. Enthalpically, the energetical affinity of NRs to A domains changes the effective A block composition (f_a), driving a series of morphological transitions. Entropically, based on the confinement from narrow phase separated domains of diblocks and the inherent anisotropy of NRs, it can be inferred that the orientational entropy of NRs and the conformational entropy of A blocks dominates the orientation behavior of NRs. As a result, by choosing appropriate L_r and ϕ_r, we can facilitate the fabrication of nanostructured composites with the desired morphologies and properties.

Additionally, in order to determine how the interactions between blocks and NRs affect the self-assembly of diblock/NR mixtures, we fix $a_{AR} = 15$, $\phi_r = 28\%$, and then calculate the phase diagram as a function of interaction strength a_{BR} and NR length L_r

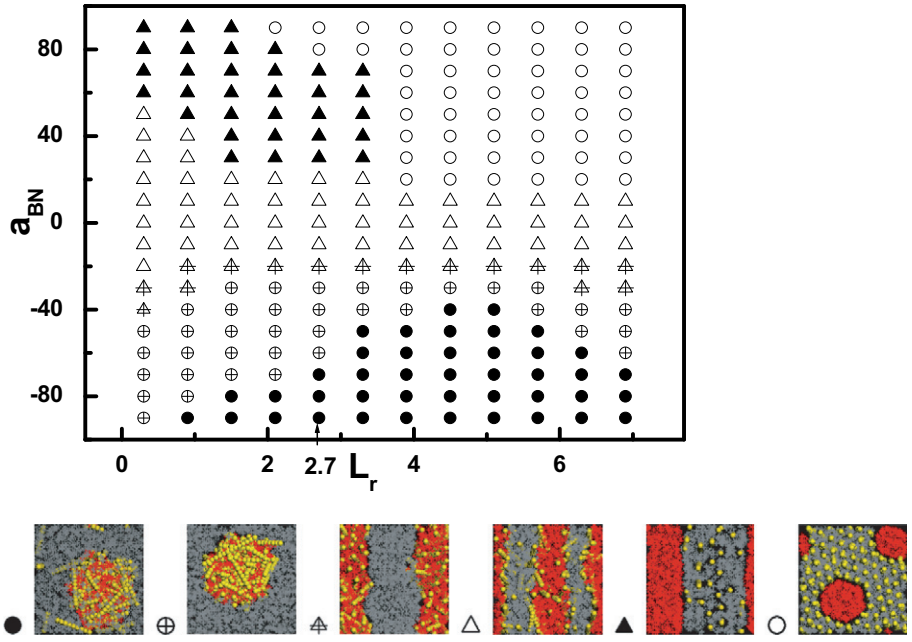

Fig. 5. The phase diagram for A_5B_5 and monodisperse NRs mixtures with different NR lengths L_r and different interaction strengths a_{BN}. Here $a_{AR} = 15$ and $\phi_r = 28\%$. Graphic symbols represent ordered morphologies: ● = S', ⊕ = C', ⏃ = $\overline{3L}$, △ = $5L$, ▲ = $3L$, and ○ = C.

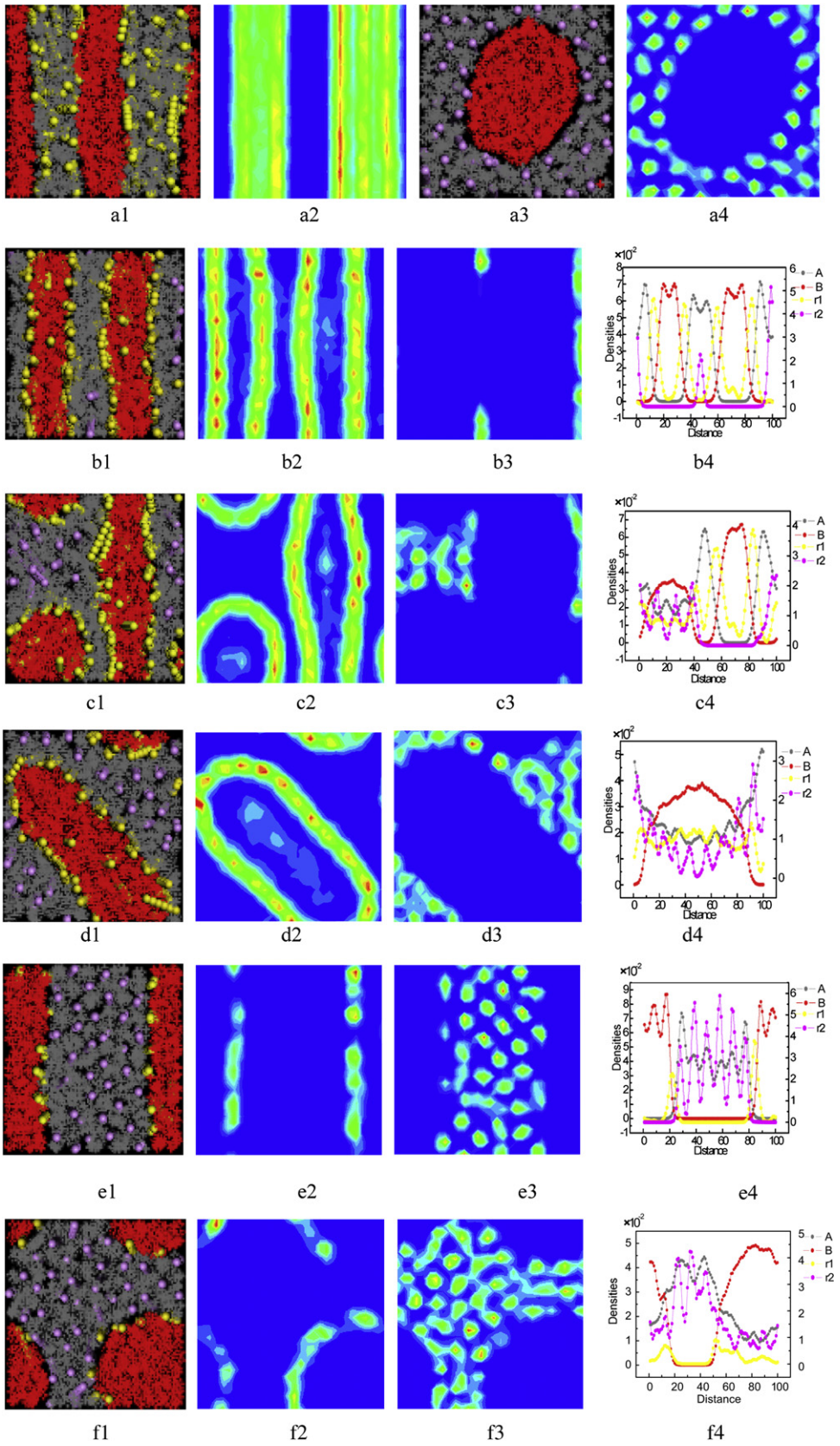

Fig. 6. Morphologies, the short NR concentrations, the long NR concentrations, and densities for A_5B_5 and bidisperse NRs mixtures. Here $a_{AR} = 15$, $a_{BR} = 20$, and $\phi_r = 28\%$. The monodisperse NRs mixtures for the short NRs ($L_{r1} = 1.5$) and the long NRs ($L_{r2} = 5.7$) are shown in (a1–a4). The bidisperse NRs mixtures for ϕ_{r1}:ϕ_{r2} = 5:1, 2:1, 1:1, 1:4 and 1:7 are shown in (b1–b4 to f1–f4). The short and long NRs are represented in yellow and purple, respectively (For interpretation of the references to colour in this figure legend, the reader is referred to the web version of this article).

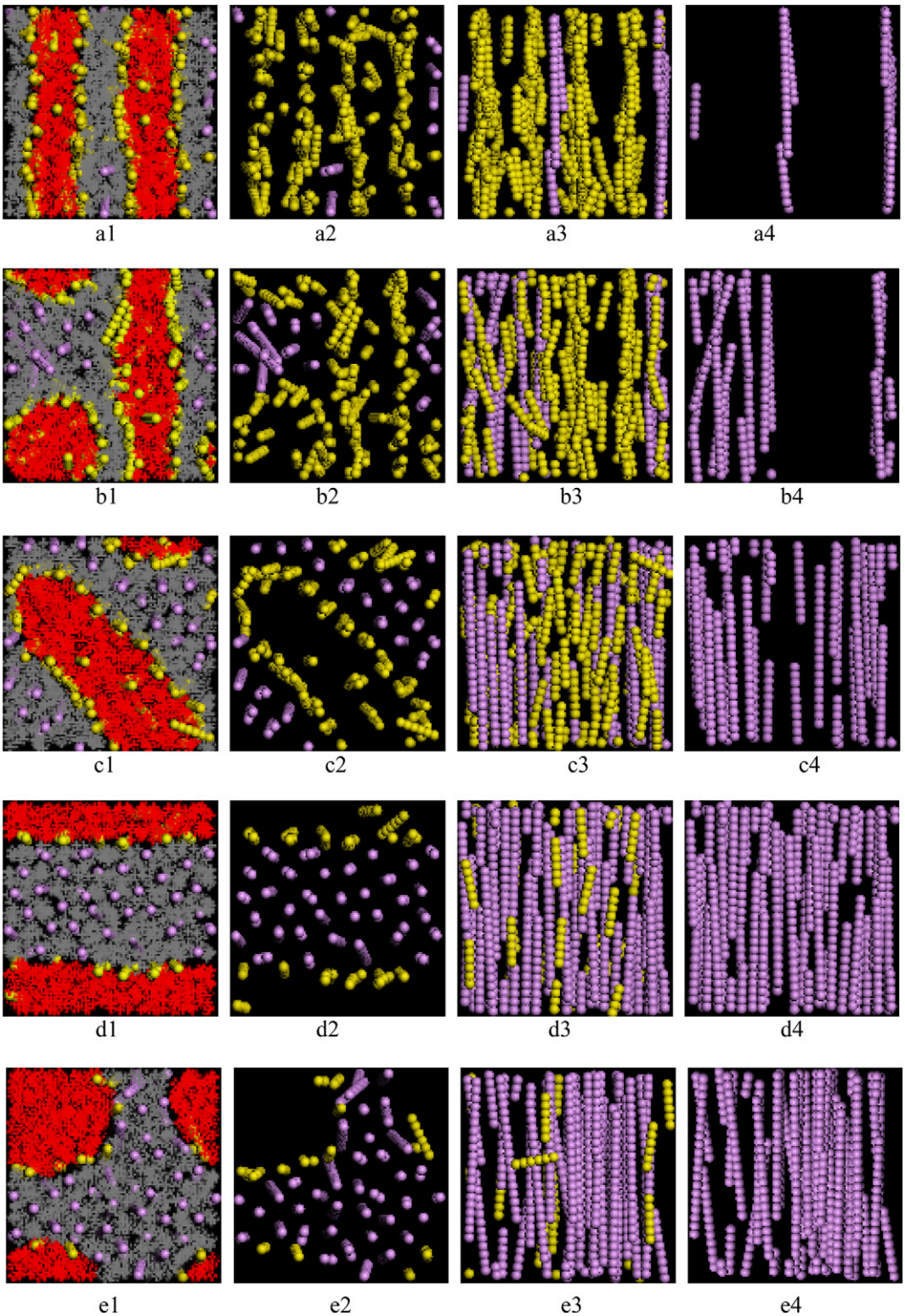

Fig. 7. Morphologies, the binary NRs distributions, the binary NRs orientations, and the long NR orientations for A_5B_5 and bidisperse NRs mixtures. All parameters are the same as in Fig. 6. The NRs orientations in (a3–e3 and a4–e4) are the side views of the NRs distributions shown in (a2–e2).

shown in Fig. 5. According to Eq. (9), the interaction strength a_{BR} between B blocks and NRs ranges from strong absorption ($a_{BR} = -90$) to strong repulsion ($a_{BR} = 90$). For the strong absorption case of $-90 \leq a_{BR} \leq -20$, there are three phases of S', C', and $\overline{3L}$ observed, respectively representing the spherical, cylindrical, two A/B interfaces lamellar structures with NRs basically located in B domains; Contrarily, for the strong repulsion case of $20 \leq a_{BR} \leq 90$, there are two main phases of $3L$, and C with NRs mainly distributed in A domains; For the intermediate case of $-10 \leq a_{BR} \leq 10$, which can be classified to the neutral NRs because of a_{BR} close to a_{AR}, the bulk lamellar structure $5L$ with NRs mainly distributed at the interface between the A and B domains, keeps unchanged for

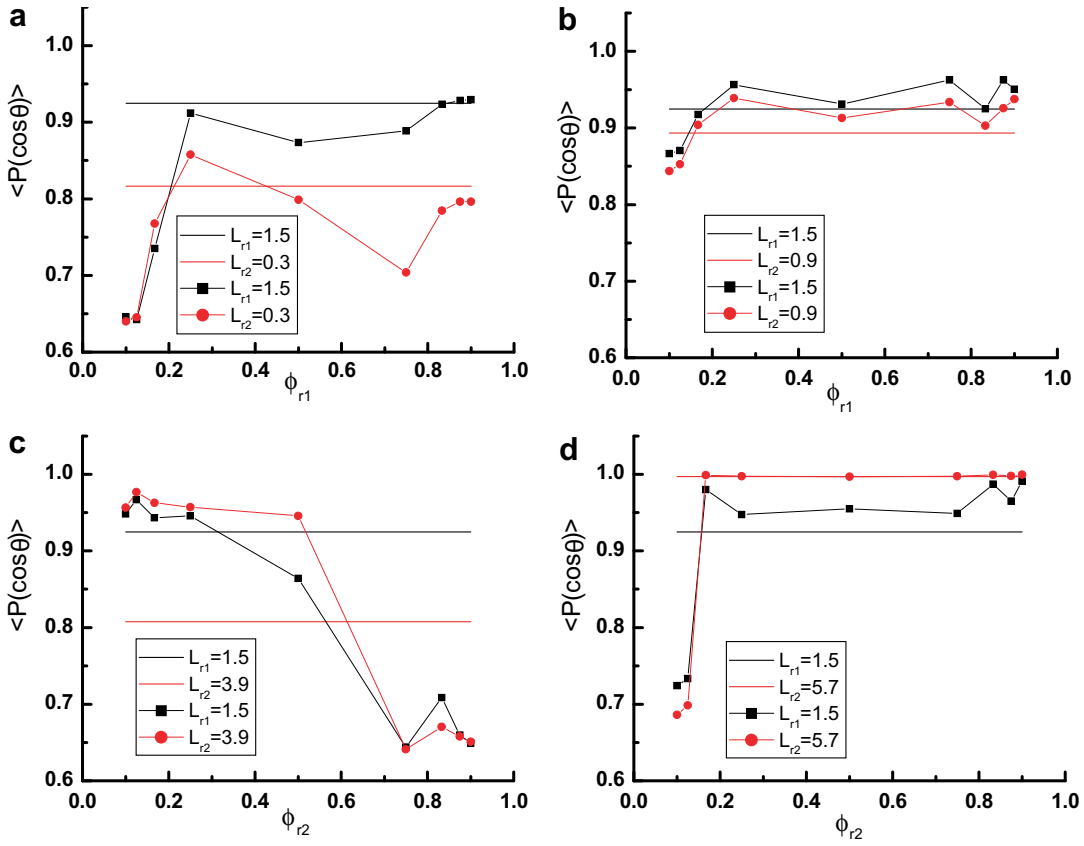

Fig. 8. Average NR orientation $<P(\cos\theta)>$ as a function of the long NRs volume fraction for A_5B_5 and bidisperse NRs mixtures with a fixed length NRs of $L_{r1} = 1.5$. In (a–b), $r1$ represents the long NRs; and in (c–d), $r2$ represents the long NRs. The lines and lines + symbols represent the mono- and bidisperse NRs mixtures, respectively.

varied NR lengths. Take the case of $L_r = 2.7$ for example, with a_{BR} varying from −90 to 90, a series of phase transitions are induced as $S' \rightarrow C' \rightarrow \overline{3L} \rightarrow 5L \rightarrow 3L \rightarrow C$, comparable with the whole theoretically predicted phase diagram with f_a varying from 0 to 1 [45]. Generally, the interactions $a_{A(B)R}$ between A/B blocks and NRs drive the distribution of NRs; conversely, the distributions of NR aggregate also direct the self-assembled phase of DBCPs.

3.2. DBCPs and bidisperse NRs mixtures

The main purpose in this report is to investigate the self-assembly of DBCPs and bidisperse NRs mixtures, in which the binary NRs are identical in energy but different in lengths. We still set $a_{AR} = 15$ and $a_{BR} = 20$, implying both types of NRs are the same preferentially wetted by A blocks. Firstly, according to the phase diagram in Fig. 3, we isolate two monodisperse NRs systems with the same NR volume fraction $\phi_r = 28\%$, and different NR lengths $L_{r1} = 1.5$(defined as short NRs) and $L_{r2} = 5.7$(defined as long NRs). From the morphologies and NR concentrations shown in Fig. 6 (a1–a4), we can clearly observe the lamellar (L) and cylindrical (C) structures with NRs concentrated at the compatible A domains, corresponding to the short and long NRs cases, respectively.

Then, we replace the monodisperse NRs with an equal volume fraction of bidisperse NRs, and change the composition of the binary NRs by varying the ratio ϕ_{r1}:ϕ_{r2}, where ϕ_{r1} and ϕ_{r2} respectively represent the volume fraction of short and long NRs in the mixtures. When ϕ_{r1}:ϕ_{r2} = 5:1, 2:1, 1:1, 1:4 and 1:7, the phase transitions are observed as follows: $5L \rightarrow L + C \rightarrow R \rightarrow 3L \rightarrow C$, where R represents the structure of ribbon shown in Fig. 6d1. The morphologies, the short NR concentrations, the long NR concentrations, and densities for A_5B_5/bidisperse NRs mixtures are shown in Fig. 6(b1–b4 to f1–f4). To tri-dimensionally observe the orientation behaviors of the binary NRs in detail, we also display the morphologies, the binary NRs' position distributions and spatial orientations, and the long NRs' spatial orientations in Fig. 7. These figures reveal a new structural feature: the same attractions to A block, but the short and long NRs are not homogeneously distributed. Now the long NRs are basically concentrated in the center of the A domains, while the short NRs are expelled to the edge of the A/B interface and, even to a small degree, in the incompatible B phase [18]. Moreover, from the NRs orientation diagrams shown in Fig. 7(a3–e3 and a4–e4), whether for the short or for the long NRs, the orientations are almost along the same direction, especially for the long NRs, whose orientations are more uniform. Thus, replacing the monodisperse NRs with an equal volume fraction of bidisperse NRs and varying the composition of the binary NRs, we can obtain not only a series of phase transformations ($5L \rightarrow L + C \rightarrow R \rightarrow 3L \rightarrow C$) in the polymer microstructure, and but also the creation of a discriminative distribution of NRs with uniform orientations. Moreover, above transformations indicate that one can drive a transition from a lamellar to a discriminative cylinder phase, as well as a reverse transition from a cylindrical to a discriminative lamellar structure through varying the relative composition (ϕ_{r1}:ϕ_{r2}) of the binary NRs. The system constitutes a discriminatively ordered nanocomposite, having an extensive application prospect. If the NRs are charged or magnetic, this amazing phase behaviors of NRs can improve greatly its opto-electronic properties in the practical application.

The inherent mechanism for driving these phase behaviors is necessary to be further exploited. Firstly, despite of the large repulsions between NRs, there is an instinctive aggregate of NRs as a result of NRs' anisotropy, and a "depletion attraction" between the

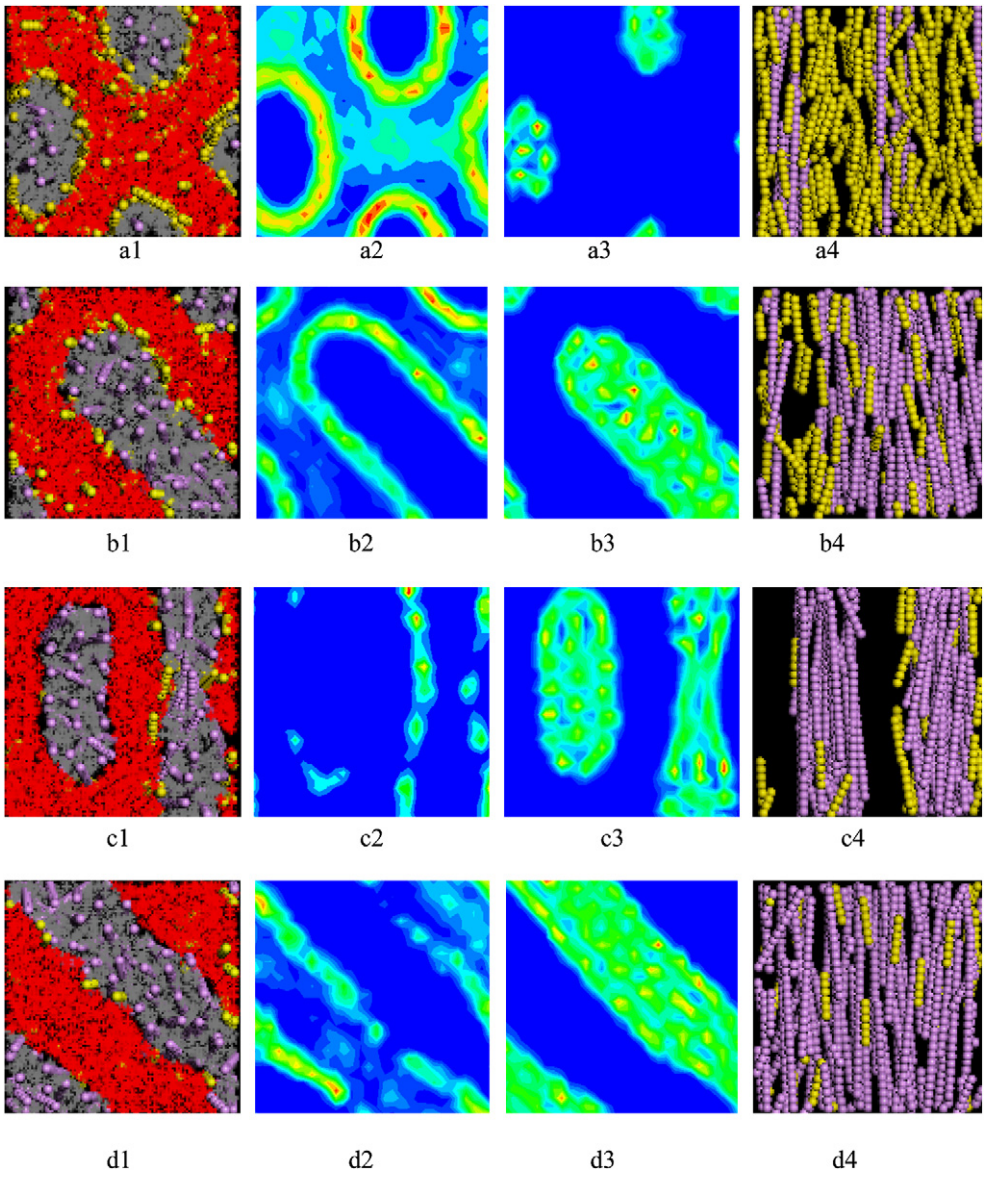

Fig. 9. Morphologies, the short NR concentrations, the long NR concentrations, and the binary NRs orientations for A_3B_7 and bidisperse NRs mixtures with ϕ_{r1}:ϕ_{r2} = 3:1, 1:2, 1:6, and 1:8, respectively. The other parameters are the same as in Fig. 6.

longer objects due to the extra volume that is available to the shorter NRs when the longer NRs approach one another [46,47]. Secondly, due to the affinity to A blocks, the long NRs are primarily located in A domains, which equivalently changes A/B block effective composition and then drives the morphological transitions. In this way, with the long NRs mainly distributed in A domains, the A chains do not lose conformational entropy by having to stretch around these large obstacles. Thirdly, due to the confinement from the phase-separating domains and the excluded volume effects from the long NRs, the short NRs are expelled to other regions including the A/B interface and incompatible B phase, which can gain the translational entropy, suggesting a "microphase separation" in the NRs system. To some extend, it can be inferred that the long NRs dominate the phase behaviors of the mixtures of diblocks and bidisperse NRs. Consequently, for the mixtures of DBCPs and the binary NRs, its self-assembly is dominated by the two contributions: the enthalpy governed by the interactions between blocks and NRs, and the entropy governed by the inherent anisotropy of NRs and the confinement from phase separated block domains.

To quantitatively investigate the orientation behaviors of the binary NRs incorporated in the copolymers, we also calculate the average NR orientation $\langle P(\cos\theta)\rangle$ versus the long NRs volume fraction for four mixtures with a fixed L_{r1} = 1.5 and the varied L_{r2} = 0.3, 0.9, 3.9, and 5.7, respectively. Fig. 8 shows that the orientation behaviors of the binary NRs affects each other in the mixtures. Moreover, for the mixtures with different NR lengths, the mutual influence between the binary NRs on the orientation exhibits quite different regularities. Corresponding to Figs. 6 and 7, we take Fig. 8(d) with L_{r1} = 1.5(short NRs) and L_{r2} = 5.7(long NRs) for example. Firstly, with a few long NRs incorporated into the mixtures, the ordered orientation for the short NRs is frustrated and presented as the low value of $\langle P(\cos\theta)\rangle$. Then, with a little increase in ϕ_{r2}, the average NR orientation $\langle P(\cos\theta)\rangle$ for both short and long NRs all increases. Upon further increase of ϕ_{r2}, the value $\langle P(\cos\theta)\rangle$ of the short NRs in bidisperse mixtures (line + symbols in

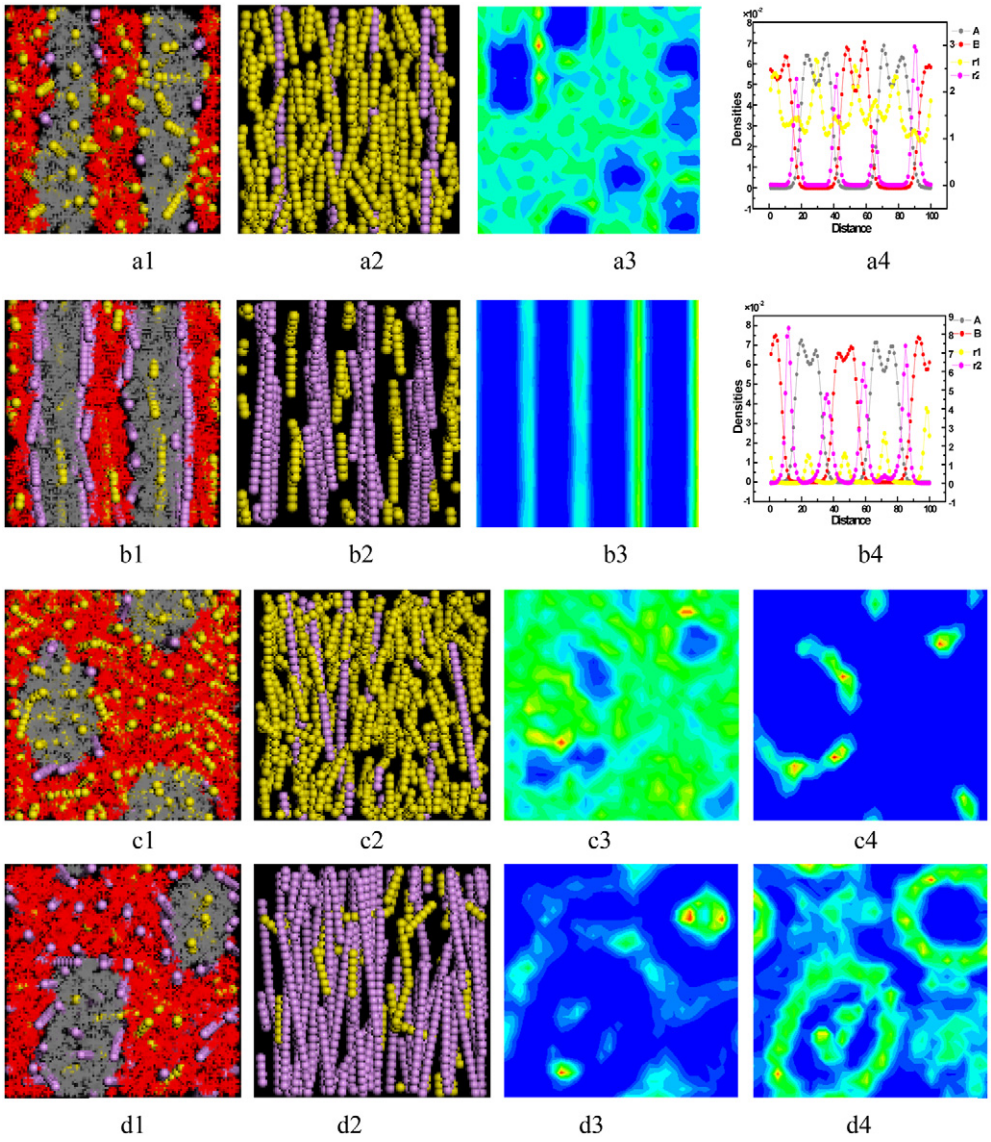

Fig. 10. For the mixtures of A_5B_5 and neutral bidisperse NRs with ϕ_{r1}:ϕ_{r2} = 4:1 and 1:4, morphologies, the binary NRs orientations, the short NR concentrations, and densities are shown in (a1–a4 and b1–b4); For the mixtures of A_3B_7 and neutral bidisperse NRs with ϕ_{r1}:ϕ_{r2} = 6:1 and 1:6, morphologies, the binary NR orientations, the short NR concentrations, the long NR concentrations are shown in (c1–c4 and d1–d4). The other parameters are the same as in Fig. 6.

black), becomes always higher than that in monodisperse case (line in black), while that of the long NRs recovers to the monodisperse case(line + symbols in red). The similar results are also observed in Fig. 8(a–b). For another case with $L_{r1} = 1.5$ and $L_{r2} = 3.9$ shown in Fig. 8(c), whether for the short or long NRs, the values of $\langle P(\cos\theta)\rangle$ all decrease as the increase of ϕ_{r2}.The results for both cases can be illustrated through the $\langle P(\cos\theta)\rangle$ curves for monodisperse NRs mixtures shown in Fig. 4, especially for L_r = 3.9 and 5.7. These observations indicate that the orientation behaviors of the binary NRs mixtures with different sizes influence each other.

Comparing with the symmetric DBCPs (A_5B_5), we also investigate the phase behaviors of the asymmetric DBCPs (A_3B_7) and bidisperse NRs mixtures. The parameters, such as NR length, NR volume fraction, and the NRs' affinity to blocks, are the same as the case of A_5B_5. In monodisperse case, the mixtures of short NRs (L_{r1} = 1.5) and long NRs (L_{r2} = 5.7) can form cylindrical (C) and lamellar (L) structures, respectively. Then, we turn to the binary NRs case, and also replace the monodisperse NRs with an equal volume fraction of bidisperse NRs. Compared to Figs. 6 and 7, the morphologies, the short NR concentrations, the long NR concentrations, and the binary NRs orientations for A_3B_7/bidisperse NRs mixtures with ϕ_{r1}:ϕ_{r2} = 3:1, 1:2, 1:6, and 1:8 are shown in Fig. 9. These observations reveal a similar results with the case of A_5B_5: a reverse structure transition $C \rightarrow R \rightarrow L + C \rightarrow 5L$ is observed in the polymer microstructure, and the binary NRs present not only a uniform orientation, but also a discriminative distribution. Since all NRs (both short and long NRs) are wetted by A blocks and are incompatible with B blocks, and there is a "depletion attraction" between the longer NRs due to the extra volume that is available to the shorter NRs, the long NRs primarily segregate in the center of the A blocks, as shown in Fig. 9(a3–d3), while the short NRs are basically expelled to the edge of the A phase, and even to a small degree into the B domains, as shown in Fig. 9(a2–d2). Apparently, it is found that this type of discriminative organization for short/long NRs is sufficiently general in the systems of symmetric/asymmetric DBCPs blended with binary NRs in which there are different in length. The same mechanism is responsible for the self-assembly as mentioned above for A_5B_5 case. The change of diblock composition can induce nanocomposites with different morphologies.

3.3. DBCPs and neutral bidisperse NRs mixtures

Finally, we consider the mixtures of symmetric/asymmetric DBCPs and neutral bidisperse NRs. Here we set $a_{AR} = a_{BR} = 15$, implying the NRs are nonselective and naturally tend to concentrate at the A/B interface. For lamellar forming A_5B_5 and neutral bidisperse NRs mixtures, the morphologies, the binary NRs orientations, the short NR concentrations, and densities are shown in Fig. 10(a1–a4 and b1–b4). Due to the nonselection for NRs to diblocks, the loading of NRs does not influence the diblock composition, hence, the system preserves the bulk lamellar (L) phase. However, despite of the nonselective interactions between blocks and NRs, the short and long NRs are not homogeneously distributed. A closer look at the NRs densities in Fig. 10(a4 and b4) reveals that the long NRs primarily occupy the A/B interface domains, while the short NRs are forced to distribute more or less uniformly over both the A and B domains, with a much lower concentration at the A/B interface. One results of the unchanged lamellar (L) structure are consistent with theoretical predictions for the behavior of the neutral NPs added to DBCPs [8], which is presumably driven by the enthalpic gain in reducing the interfacial tension, γ, between the A and B blocks. The other results of the discriminative distributions of the binary NRs mainly result from the cooperative competitions between the conformational entropy of blocks and orientational entropy of NRs. For the cylindrical forming A_3B_7 and neutral bidisperse NRs mixtures, the similar results are observed in Fig. 10(c1–c4 and d1–d4): the cylindrical (C) morphology remains unchanged, and the binary NRs present a discriminative distribution. In the same manner, the long NRs preferentially fill with the A/B interface, entropically forcing the redundant NRs (both short and long) to distribute uniformly in both the A and B domains. As a result, though the neutral NRs almost have no effect on the morphology of the copolymers, the ordering of the copolymers templates the spatial organization of NRs.

4. Conclusions

We use the DPD method to investigate the self-assembly behaviors of symmetric/asymmetric DBCPs blended with mono- or bidisperse NRs. For the monodisperse NRs, we focus on the symmetric DBCPs melts blended with A-preferential NRs, and present the effects of the NR volume fraction, NR length, and interaction strength between blocks and NRs on the self-assembly of the composites. It is found that these parameters not only affect the general morphology of the mixtures but also directly influence the orientation behaviors of NRs in microphase-separated DBCPs. In this report, we mainly investigate the DBCPs (symmetric/asymmetric) melts blended with bidisperse A-preferential NRs, in which the binary NRs are identical in energy but different in length. Replacing the monodisperse NRs with an equal volume fraction of bidisperse NRs and then varying the composition of the binary NRs, can prompt not only a series of phase transformations in the polymer microstructure, but also the creation of a uniform orientation, and a discriminative distribution of NRs. This discriminatively size-selective organization for short/long NRs is sufficiently general in symmetric/asymmetric DBCPs. Meanwhile the orientation behaviors of the binary NRs with different lengths influence each other. In the case of the neutral bidisperse NRs with varying the composition, the unchanged phase-separated DBCPs structures containing the inhomogeneous distribution of NRs are observed. The longer NRs primarily occupy the A/B interface domains, while the shorter NRs are forced to distribute more or less uniformly over both the A and B domains, with a much lower concentration at the A/B interface. The inherent mechanism for driving such rich phase behaviors can be further exploited on the basis of considering the enthalpic and entropic effects. Entropic and enthalpic interactions between blocks and NRs(especially the longer NRs), and the steric effects between the different NRs, drive the longer NRs to primarily localize in the center of the preferential blocks or the A/B interface domains, corresponding to the preferential and neutral bidisperse NRs, respectively. However, the shorter NRs can gain translational entropy by migrating into the unfavorable phase, leading to a “microphase separation” in the NRs system. In summary, the enthalpy is governed by the interactions between blocks and NRs, and the entropy is governed by the inherent anisotropy of NRs and the confinement from phase separated block domains. Overall, the studies of these rich morphologies and behaviors from various diblock/NR mixtures can offer valuable assistance in exploring and designing hybrid materials with the desired properties and morphologies.

Acknowledgements

This research was financially supported by the National Natural Science Foundation of China (Nos. 20774066, 20974081, 20934004), the Program for New Century Excellent Talents in University (NCET-05-0538), the National Basic Research Program of China (No. 2005CB623800), and the Natural Science Foundation of Zhejiang Province (No. Y4080098). We also thank the referees for their critical reading of the manuscript and their good ideas.

References

[1] Stupp SI, Braun PV. Science 1997;277:1242.
[2] Fink Y, Urbas AM, Bawendi MG, Joannopoulos JD, Thomas EL. J Lightwave Technol 1999;17:1963.
[3] Jeoung E, Galow TH, Schotter J, Bal M, Ursache A, Tuominen M, et al. Langmuir 2001;17:6396.
[4] Lopes WA, Jaeger HM. Nature (London) 2001;414:735.
[5] Lauter-Pasyuk V, Lauter HJ, Ausserre D, Gallot Y, Cabuil V, Kornilov EI, et al. Physica B 1997;241:1092.
[6] Lee JY, Shou Z, Balazs AC. Phys Rev Lett 2003;91:136103.
[7] Lin Y, Böker A, He J, Sill K, Xiang H, Abetz C, et al. Nature (London) 2005;434:55.
[8] Lee JY, Thompson R, Jasnow D, Balazs AC. Macromolecules 2002;35:4855.
[9] Sun YS, Jeng US, Liang KS, Yeh SW, Wei KH. Polymer 2006;47:1101.
[10] Kim BJ, Chiu JJ, Yi GR, Pine DJ, Kramer EJ. Adv Mat 2005;17:2618.
[11] Yeh SW, Wei KH, Sun YS, Jeng US, Liang KS. Macromolecules 2005;38:6559.
[12] He LL, Zhang LX, Liang HJ. J Phys Chem B 2008;112:4194.
[13] Maly M, Posocco P, Pricl S, Fermeglia M. Ind Eng Chem Res 2008;47:5023.
[14] Lin IH, Kuo SW, Chang FC. Polymer 2009;50:5276.
[15] Thompson RB, Ginzburg VV, Matsen MW, Balazs AC. Science 2001;292:2469.
[16] Thompson RB, Ginzburg VV, Matsen MW, Balazs AC. Macromolecules 2002;35:1060.
[17] Pryamitsyn V, Ganesan V. Macromolecules 2006;39:8499.
[18] Lee JY, Thompson RB, Jasnow D, Balazs AC. Phys Rev Lett 2002;89:5503.
[19] Lee JY, Thompson RB, Jasnow D, Balazs AC. Faraday Discuss 2003;123:121.
[20] Lee JY, Thompson RB, Jasnow D, Balazs AC. Phys Rev E 2002;66::031801.
[21] Bockstaller MR, Thomas EL. Phys Rev Lett 2004;93:166106.
[22] Bockstaller MR, Lapetnikov Y, Margel S, Thomas EL. J Am Chem Soc 2003;125:5276.
[23] Spontak RJ, Shankar R, Bowman MK, Krishnan AS, Hamersky MW, Samseth J, et al. Nano Lett 2006;6:2115.
[24] Huh J, Ginzburg VV, Balazs AC. Macromolecules 2000;33:8085.
[25] Liu D, Zhong CL. Macromol Rapid Commun 2006;27:458.
[26] Zhang QL, Gupta S, Emrick T, Russell TP. J Am Chem Soc 2006;128:3898.
[27] Li CP, Yeh SW, Chang HC, Huang JY, Wei KH. Small 2006;2:359.
[28] Ranjan D, Liu Y, Russell JC. Nano Lett 2007;7:3662.
[29] Bećneut K, Constantin D, Davidson P, Dessombz A, Chanećac C. Langmuir 2008;24:8205.
[30] Peng G, Qiu F, Ginzburg VV, Jasnow D, Balazs AC. Science 2000;288:1802.
[31] Buxton GA, Balazs AC. Mol Simul 2004;30:249.
[32] Chen K, Ma YQ. J Chem Phys 2002;116:7783.
[33] He LL, Zhang LX, Xia AG, Liang HJ. J Chem Phys 2009;130:144907.
[34] He LL, Zhang LX, Chen HP, Liang HJ. Polymer 2009;50:3403.
[35] de Gennes PG, Prost J. The physics of liquid crystals. Oxford: Oxford University Press; 1993.
[36] Adams M, Dogic Z, Keller SL, Fraden S. Nature (London) 1998;393:349.
[37] Tu YF, Graham MJ, Van Horn RM, Chen E, Fan XH, Chen XF, et al. Polymer 2009;50:5170.
[38] Buxton GA, Balazs AC. J Chem Phys 2002;117:7649.

[39] Hoogerbrugge PJ, Koelman JMVA. Europhys Lett 1992;19:155.
[40] Espanol P. Europhys Lett 1997;40:631.
[41] Groot RD, Madden TJ. J Chem Phys 1998;108:8713.
[42] AlSunaidi BA, den Otter WK, Clarke JHR. Phil Trans R Soc London A 2004; 362:1773.
[43] Hore MJA, Laradji M. J Chem Phys 2008;128:054901.
[44] Hore MJA, Laradji M. J Chem Phys 2007;126:244903.
[45] Matsen MW, Bates FS. Macromolecules 1996;29:1091.
[46] Dinsmore AD, Yodh AG, Pine DJ. Phys Rev E 1995;52:4045.
[47] Dinsmore AD, Yodh AG, Pine DJ. Nature(London) 1996;383:239.